

Multifunction Tunable Piezoelectric-Actuated Metasurface at Millimeter-Waves

Vassos, Evangelos; Feresidis, Alexandros

DOI:

[10.1002/adpr.202300109](https://doi.org/10.1002/adpr.202300109)

License:

Creative Commons: Attribution (CC BY)

Document Version

Publisher's PDF, also known as Version of record

Citation for published version (Harvard):

Vassos, E & Feresidis, A 2023, 'Multifunction Tunable Piezoelectric-Actuated Metasurface at Millimeter-Waves', *Advanced Photonics Research*. <https://doi.org/10.1002/adpr.202300109>

[Link to publication on Research at Birmingham portal](#)

General rights

Unless a licence is specified above, all rights (including copyright and moral rights) in this document are retained by the authors and/or the copyright holders. The express permission of the copyright holder must be obtained for any use of this material other than for purposes permitted by law.

- Users may freely distribute the URL that is used to identify this publication.
- Users may download and/or print one copy of the publication from the University of Birmingham research portal for the purpose of private study or non-commercial research.
- User may use extracts from the document in line with the concept of 'fair dealing' under the Copyright, Designs and Patents Act 1988 (?)
- Users may not further distribute the material nor use it for the purposes of commercial gain.

Where a licence is displayed above, please note the terms and conditions of the licence govern your use of this document.

When citing, please reference the published version.

Take down policy

While the University of Birmingham exercises care and attention in making items available there are rare occasions when an item has been uploaded in error or has been deemed to be commercially or otherwise sensitive.

If you believe that this is the case for this document, please contact UBIRA@lists.bham.ac.uk providing details and we will remove access to the work immediately and investigate.

Multifunction Tunable Piezoelectric-Actuated Metasurface at Millimeter-Waves

Evangelos Vassos* and Alexandros Feresidis

Free space (also termed quasi-optical) metasurfaces have recently been designed and proposed as new types of polarizers that allow polarization control of an impinging wave in ways that are not possible with conventional designs. However, existing methods for tunable metasurface polarizers are not able to fully control the polarization dynamically; additionally, at mm-wave and sub-millimeter bands, they typically suffer from high losses, which are predominantly produced by the inherent limitations of the tuning elements or materials. An electromechanically tunable reflection polariser that has the ability to fully control the polarization of an impinging wave has been designed, fabricated, and experimentally tested in a frequency band centered at 57 GHz. The proposed technique utilizes a variable air cavity between a periodic metasurface array and a ground plane, controlled by a piezoelectric actuator. The periodic metasurface element consists of two slightly different cross-shaped metallic elements arranged in a periodic triangular lattice. Full-wave simulations are presented and experimentally validated with measurements. The proposed approach is scalable from microwave up to THz frequencies with low-loss performance due to the nature of the tuning technology whereby the tuning element is not interfering with the electromagnetic waves in the structure.

1. Introduction

Metasurfaces are a technological breakthrough that has proliferated in recent years, with a range of applications in sensing, imaging, and communication systems. Metasurfaces are thin, low-profile versions of metamaterials that can manipulate the incident electromagnetic waves.^[1–3] Metasurfaces consist of subwavelength metallic elements arranged on a periodic (or quasi-periodic) lattice or subwavelength apertures in a metallic sheet. These novel two-dimensional structures have been used recently for various applications such as controlling the polarization state of incident waves in the


millimeter wave,^[4,5] IR/optical,^[6] propagating mode to surface mode conversion,^[7] anomalous reflection,^[8] reflectarray antennas,^[9–11] absorbers,^[12–14] high-impedance surface-based antennas,^[15] reflectors,^[16] transmitarrays,^[17–19] and cloaking.^[20,21] Furthermore, metasurfaces have been proposed that possess the capability to perform multiple functions, such as the independent control of horizontal and vertical polarizations for reflectarray or transmitarray applications^[22] and/or amplitude and phase control.^[23] An additional advantage of metasurfaces is that they can be scaled from millimeter frequencies up to the THz regime or even the infrared spectrum,^[24] depending on the design and fabrication capabilities.

A key factor in the development of novel metasurfaces is the capability to dynamically control the impinging electromagnetic wave by applying a tuning method. Some of the tuning technologies that have been proposed are ferroelectric substrates,^[25] liquid crystals,^[26,27] phase change materials such as vanadium dioxide,^[28] graphene,^[3,29] diodes,^[30–33] microelectromechanical systems (MEMS),^[34,35] and more recently piezoelectric actuators (PEAs).^[36,37] The choice of tuning method depends on the application and the required performance parameters. Basic parameters that normally guide the choice of the appropriate tuning method are the frequency of operation, loss tolerance, switching/tuning speed, ease of integration, form factor, cost, etc.

In the case of applications where polarization control of the impinging electromagnetic wave is required, the essential parameters are continuous phase control of the two orthogonal components of the electromagnetic wave, low losses, low profile, and a satisfactory operating range. For example, in the case of satellite communications systems, polarization control is required due to the rotational movement of satellites.^[38]

In addition, a structure where it can force alternations between the polarization states without the necessary use of multiple antennas can lead to a drastic reduction in satellite costs. A particular application is the satellite polarimetric imaging systems that include channels for receiving and sending a different polarization state.^[39] The main uses of these systems are the passive or active monitoring of the velocity of the air at the earth's surface and the collection of vegetation information.^[40] The dynamic change in the polarization state could enhance radar systems' detection and measurement of a target/object.^[41] In addition,

E. Vassos, A. Feresidis
Department of Electronic, Electrical and Systems Engineering
University of Birmingham
Birmingham B15 2TT, UK
E-mail: e.vassos@bham.ac.uk

 The ORCID identification number(s) for the author(s) of this article can be found under <https://doi.org/10.1002/adpr.202300109>.

© 2023 The Authors. Advanced Photonics Research published by Wiley-VCH GmbH. This is an open access article under the terms of the Creative Commons Attribution License, which permits use, distribution and reproduction in any medium, provided the original work is properly cited.

DOI: 10.1002/adpr.202300109

flexibility in the polarization state can be included in millimeter systems for isolation,^[42] filtering, and diplexing.^[43] The requirements of modern advanced driving assistant systems include the reliable characterization of targets to analyze complex scenarios.^[41] Reconfigurable polarizers could also characterize their targets compared to single or dual-polarized radars.^[44]

In recent years, devices that can partially control the polarization state of an electromagnetic wave have been reported in the literature. The initial polarization conversion structures were based on mechanical motors or rotors, with additional disadvantages of high energy consumption, relatively slow response, bulky design, and reduced reliability.^[41] To solve the disadvantages mentioned above, MEMS^[45] and piezoelectric ultrasonic motors^[46] were introduced. Due to the small size of the mechanisms, they succeeded in improving the reconfigurable polarizers; however, it was impossible to use these mechanisms for dynamic control of polarization, except for a discrete change of the polarization state. These tuning mechanisms mentioned above refer to waveguide-based polarizers' applications, and it is not easy to scale them to higher frequencies due to the dimensions of the specific mechanisms.

Free-space/quasi-optical structures introduce more challenges due to the larger size (several wavelengths) and higher number of tuning elements. A free-space reconfigurable reflection polarizer

with a liquid crystal tuning mechanism was reported recently.^[47] Despite their growing use in various applications, liquid crystals exhibit higher losses and switching speeds ranging from a few milliseconds to several seconds, which can limit their performance^[48,49]

This manuscript presents a novel metasurface that can fully control the phase and polarization of an electromagnetic incident wave. The structure consists of a periodic array printed on a dielectric substrate. The ground plane is positioned at a certain distance from the dielectric, creating an air gap, as shown in **Figure 1**. An advantage of this unconventional configuration is the significant reduction of reflection losses and increase of the operating bandwidth. Introducing a tuning method in this design adds an extra degree of freedom to control the reflection response. A piezoelectric actuator is placed under the ground plane, as shown in Figure 1a, with the direction of motion (displacement) along the z axis. Since the mechanism is placed under the ground plane, its device does not interfere with the electromagnetic wave above the ground plane. The outcome of the aforementioned technique is a reduction in losses, and it has been previously employed in structures incorporating piezoelectric actuators^[36] and electronic components.^[50] Based on the piezoelectric mechanism's properties, the ground plane's position can be controlled precisely (in the order of nm) with a

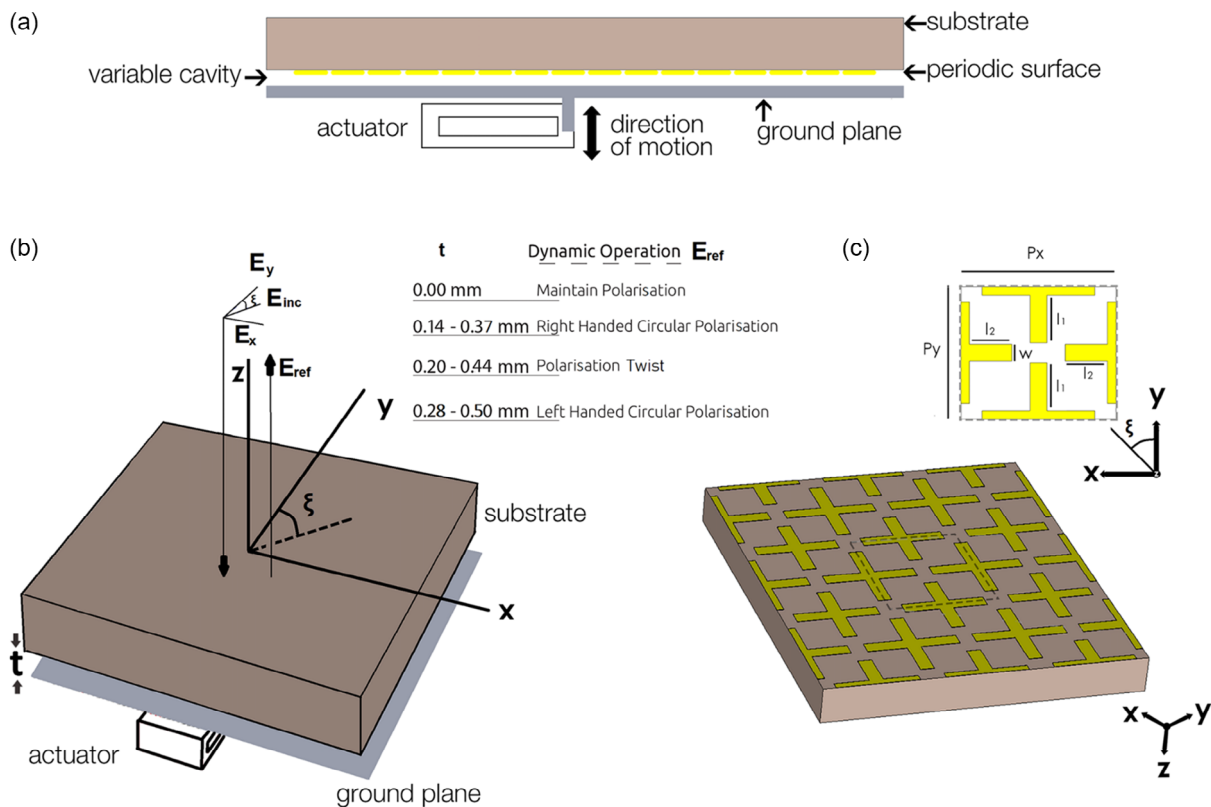


Figure 1. A schematic of the proposed piezoelectric-actuator-controlled reflection metasurface polarizer. a) Schematic illustration of the cross-section of the polarizer, highlighting the unconventional configuration with an air cavity between the ground plane and the periodic array. The ground plane is controlled by applying a voltage to the piezoelectric actuator resulting in micromovement of the ground plane along the z-axis. b) Schematic illustration of the proposed reconfigurable polarizer that highlights its four functions corresponding to different ground plane positions. c) The periodic metasurface array consists of crosses printed on a Nelco NY9220ST0787S1S1 dielectric with a thickness of 0.78 mm. The anisotropy arises from the slightly different dimensions of the two crosses of the periodic unit cell and their relative position.

switching speed in the order of milliseconds. Additionally, we can bring the ground plane in contact with the periodic structure and separate them dynamically (i.e., continuously) up to a maximum displacement/separation of 0.5 mm. The contact of the periodic elements with the ground plane entails the cancellation of the operation of the metasurface. In addition, the small thickness of the air cavity maximizes the influence of the movement of the ground plane. The anisotropic design of the metasurface unit cell makes it possible to independently control the reflection characteristics of the two orthogonal linearly polarized incident plane waves and, therefore, achieve linear to right or left circular polarization or the twist of the linear polarization by 90°.

2. Results and Discussion

2.1. Multifunction Metasurface

The reconfigurable polarizer's operation is demonstrated by a structure designed to operate at a central frequency of around 57 GHz and different bandwidths depending on the operation of the structure. The dielectric chosen for this application is the Nelco NY9220ST0787S1S1 with a thickness of 0.78 mm (dielectric constant 2.2 and loss tangent 0.0009). The metasurface consists of a periodic array of anisotropic (with respect to the x and y axes) cross-shaped metal elements. Each unit cell consists of two slightly differentiated crosses placed in triangular lattice symmetry, as shown in Figure 1b, where $P_x = 2.75$ mm, $P_y = 2.35$ mm, $l_1 = 0.85$ mm, $l_2 = 0.75$ mm, and $w = 0.30$ mm. Due to the periodic nature of the metasurface, and after applying Floquet periodic boundary conditions, the whole structure can be studied simply by simulating the unit cell. Without losing any information about the design and for the best use of time and computing power, only the unit cell was simulated in the CST microwave studio. The effect of the piezoelectric actuator was inserted in the simulated model as a movable ground plane, without the presence of the actuator itself, since the mechanism is placed under the ground plane and does not interfere with the electromagnetic wave above the ground plane.

The anisotropic design of the unit cell creates the conditions for the differentiated behavior of the two orthogonal components of the incident wave. In this case, the anisotropy derives from the orthogonal shape of the unit cell ($P_x > P_y$) combined with the triangular lattice symmetry of the two slightly differentiated crosses. The incident and reflected waves are expanded into two orthogonal linearly polarized waves along x and y and are commonly referred to as T_E and T_M polarizations, respectively. The metasurface's control focuses on the phase difference between the T_E and T_M polarized components. This phase difference will allow the incident linear polarization to be converted to the desired polarization. In addition, it should be noted that both orthogonal components of the reflected wave must have similar amplitude. Different reflection losses between the two orthogonal components could prevent complete conversion or twist of the polarization state.

To extract the results for the polarization of the reflected wave, the orthogonal components were studied independently. The simulated results suggest that a conversion from linear polarization to circular polarization can be accomplished, as well as

preservation or a 90° twist of the linear polarization of the incident wave by moving the ground plane. It should also be noted that different frequencies may require different air cavity heights to achieve conversion to any of the above polarization states.

2.1.1. Polarization Twist

Initially, a study was conducted for the twist of the polarization by 90°. We observed that for a distance between the array and the ground plane from 0.2 to 0.44 mm, there is a dynamic reversal of the polarization for an incident electromagnetic wave, with angle $\xi = 45^\circ$ with respect to the y -axis, as shown in Figure 1b. The first condition to twist the polarization of the incident wave by 90° is for the phase difference of the two reflected orthogonal components to be 180°.^[51] The second condition is that the losses of the two reflected orthogonal components should be equal. The two orthogonal components were studied separately to confirm the phase difference between them. The results are shown in Figure 2a,b, where it is apparent that the requirements for polarization inversion are satisfied.

The simulated results suggest a polarization twist of 90° for a dynamic operating range from 53.8 to 61.0 GHz (Figure 2a). The operating range was determined for the movement of the ground plane from 0.20 to 0.44 mm. This movement is continuous, dynamic, and precise due to the capabilities of the piezoelectric mechanism that holds and moves the ground plane. The magnitude of the 90° twisted reflected wave is shown in Figure 2b indicating reflection losses of less than 10% of the whole operating frequency range.

2.1.2. Right-Handed Circular Polarization

The subsequent study examined whether the structure could convert linear to right-handed circular polarization. The criteria for the incident electromagnetic wave with linearity $\xi = 45^\circ$ with respect to the y -axis to be reflected having right-handed polarization are for its orthogonal components: a) to have a phase difference of 90° and b) to have similar reflection losses.^[52] The axial ratio of the structure was calculated from the simulation results obtained for the two orthogonal components of the reflected electromagnetic field.^[53] The simulation results are presented in Figure 2c,d, where we have the conversion from linear to right-handed circular polarization based on the phase difference of the two orthogonal components. As suggested by the simulations, the right-handed circular polarization is observed for a cavity height from 0.14 to 0.37 mm for a dynamic operating bandwidth from 53.8 to 61 GHz. The 3 dB-axial ratio bandwidth is at least 0.5 GHz for the various positions of the ground plane. As in the previous study, the reflection losses of both components are less than 1.5 dB in the whole operating bandwidth.

2.1.3. Left-Handed Circular Polarization

In this case, the requirements to convert the linear polarization to left-handed circular polarization for an incident electromagnetic wave with linearity ξ of 45° to the y -axis are a) the orthogonal components of the reflected electromagnetic wave must have a phase difference of 270° as well as b) similar reflection

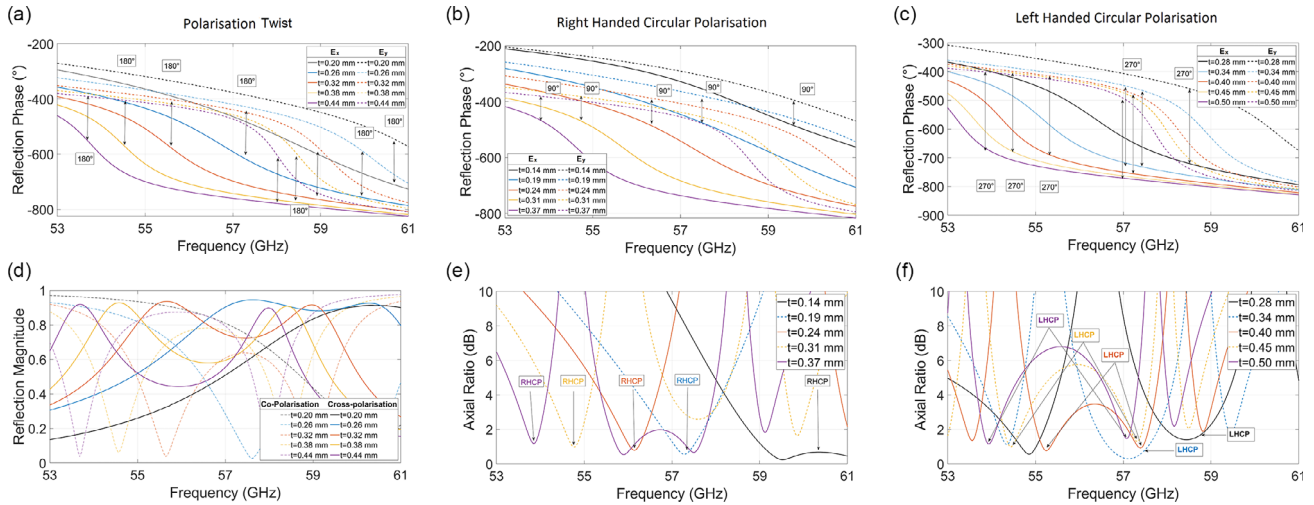


Figure 2. Simulation results of the reflection phase difference between the two orthogonal components of an electromagnetic wave that interacts with the proposed dual cross element when the parameter t varies. a) Presents the phase difference of 180° in the whole spectrum between the two orthogonal components for an air cavity between 0.20 and 0.44 mm. b) Presents the co- and cross-polarization when the impinging wave has a linearity of 45° , where is highlighted the rotation of the linear polarization by 90° for the corresponding cavity height. c) The phase difference of 90° between the two orthogonal components, which is a requirement for the RHCP, is presented for positions of the ground plane between 0.14 and 0.37 mm. d) The axial ratio of the reflected wave is given for the corresponding ground plane positions. e) The phase difference of 270° between the two orthogonal components, which is required for the LHCP, is presented for cavity heights between 0.28 and 0.50 mm. f) The axial ratio for the corresponding positions of the ground plane is presented.

losses.^[52] The simulated reflection phase and the axial ratio are shown in Figure 2e,f. The cavity height varies from 0.28 to 0.50 mm. The reflection losses remain below 1.5 dB, and we have a phase difference of 270° between the two orthogonal components. Following the previous study, the axial ratio was calculated similarly from the simulated results of the two orthogonal components. The operating range for a 3 dB axial ratio is from 53.8 to 59 GHz. The conditions are met to convert the polarization from linear to left-handed circular with a minimum 3 dB axial ratio bandwidth of 0.5 GHz.

2.1.4. Preservation of Linear Polarization

The final characteristic of the device is the linear polarization maintenance. The piezoelectric actuator can bring the periodic array in contact with the ground plane, which results in the elimination of the microcavity. We can observe that the electromagnetic wave incident on the metasurface is reflected with minimal losses while maintaining its polarization, as it would on a flat metal surface. The preservation of the linear polarization exceeds the operating bandwidth of the structure.

2.1.5. Surface Currents Distribution Analysis

Figure 3a–d presents the surface current distribution at 57 GHz for different positions (0.00, 0.19, 0.26, and 0.34 mm) of the ground plane when an electromagnetic wave with a linearity of 45° is incident, which for the specific frequency gives us the four separate functions of the structure. Initially, in Figure 3a, we have observed that very low currents as the periodic array is grounded. In this case, we have the reflection of the electromagnetic wave without any conversion of the initial

polarization with almost zero losses. In the other three Figure 3b,c,d, the maximum current amplitude is around the crosses. As we move the ground plane away from the periodic array we notice that the maximum current value decreases. The maximum surface current value in the case of right-handed circular polarization is 6485.5 A m^{-1} which happens for a 0.19 mm air cavity height. For the air cavity with a height of 0.26 mm, where we obtain the twist of the linear polarization, we have a maximum current value of 4846.7 A m^{-1} . Finally, we observe that we have 118.3 A m^{-1} for an air cavity with a height of 0.34 mm, which corresponds to the case of left-handed circular polarization. As the distance between the ground plane and the periodic array decreases, we have weaker surface currents that lead to lower reflection losses for the same frequency. The currents, in all cases, diffuse evenly along the x and y axes.

2.2. Phase Shifter Operation for X- and Y-Polarizations Separately

Another functionality of this polarization converter is to obtain a relatively large reflection phase shift of more than 360° ^[35] for each of the two orthogonal components, x or y . To achieve this phase shift range, two resonances must be generated from the structure at a short frequency distance. The two resonances should have the same amplitude otherwise, one of them becomes quite sharp. This study also has a direct impact on the design presented in the previous sections. For example, if we have a sharp resonance, the difficulty in converting the polarization increases as we introduce more reflection losses to one of the two orthogonal components which can lead to an imbalance in terms of the amplitude of the two electric field components. We can adjust the frequency separation of the two resonances by

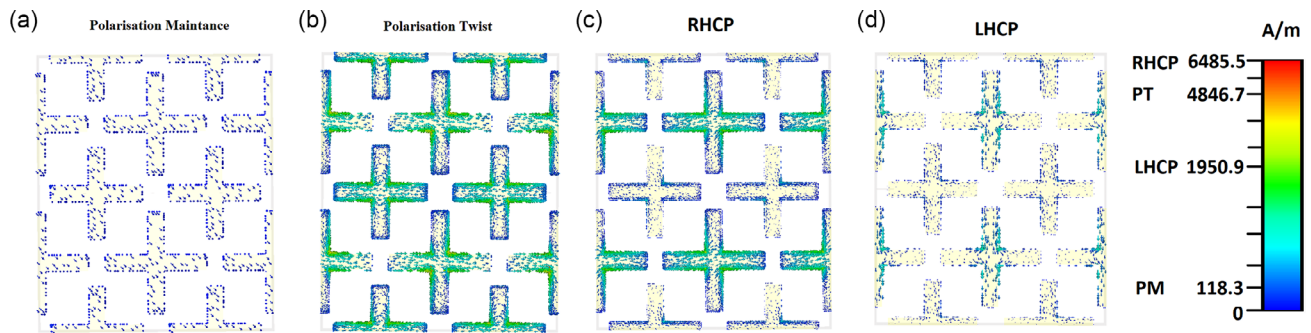


Figure 3. Surface currents distribution analysis. The surface currents for four different positions of the ground plane (0.00, 0.19, 0.26, and 0.34 mm) at 57 GHz. The aforementioned four positions represent the four functions of the structure when interacting with an electromagnetic wave with a linearity of 45°. Where a) corresponds to the polarization maintenance, b) to the polarization twist, c) to right-handed circular polarization, and d) to left-handed circular polarization. As the distance between the ground plane and the periodic array decreases, we have weaker surface currents that lead to lower reflection losses for the same frequency.

changing the geometric dimensions of the crosses. Another critical parameter is that as we increase the air cavity height between the periodic structure and the ground plane, we shift both resonances to a lower frequency. The electrical length of the two crosses at a lower frequency approaches each other, resulting in a single resonance.

Following the above designing parameters, we extract the results shown in **Figure 4a–d**. For the ground plane moving from 0.10 mm to 0.50 mm for the x-polarization, we have a 57 GHz phase shift of 530°, while for the y-polarization, we have 270° at the same frequency. The maximum phase shift value of 493° for the y-polarization is at 60 GHz. In addition, we observe

that for all ground plane positions and for both polarizations in the frequencies of interest, the reflection losses are less than 1.5 dB, and their amplitudes are similar.

2.3. Angular Stability Study

Extensive studies have been performed on the angular stability of the device and are presented in **Figure 5**. Initially, the studies were performed for changes in the angles of incidence θ_{zx} and θ_{zy} with respect to the z-axis defined in Figure 5a,b with a constant cavity height between the ground plane and the periodic array. For each PT, RHCP, and LHCP function, the cavity

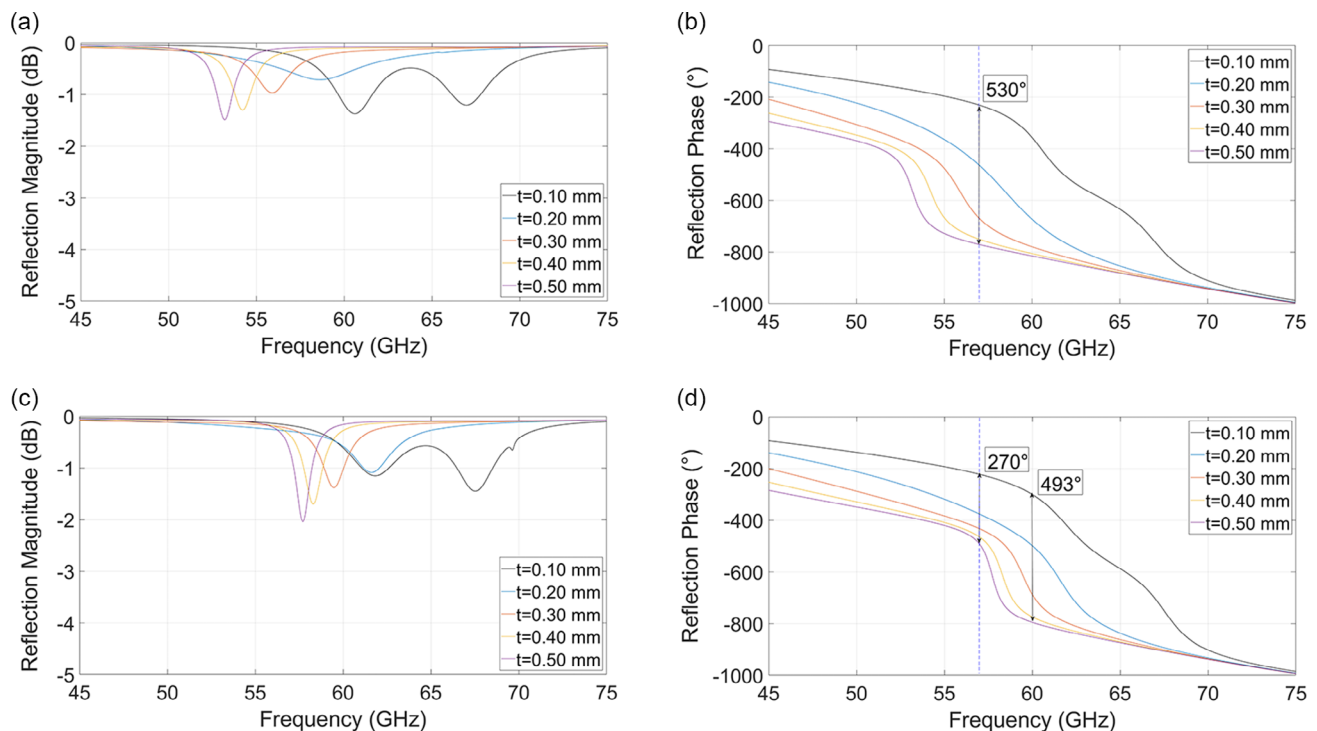


Figure 4. Design analysis. Simulation results of the a) reflection magnitude and the b) reflection phase of the proposed double-cross element for the x-polarization. The reflection magnitude c) and the phase shift d) for the y-polarization by varying the parameter t .

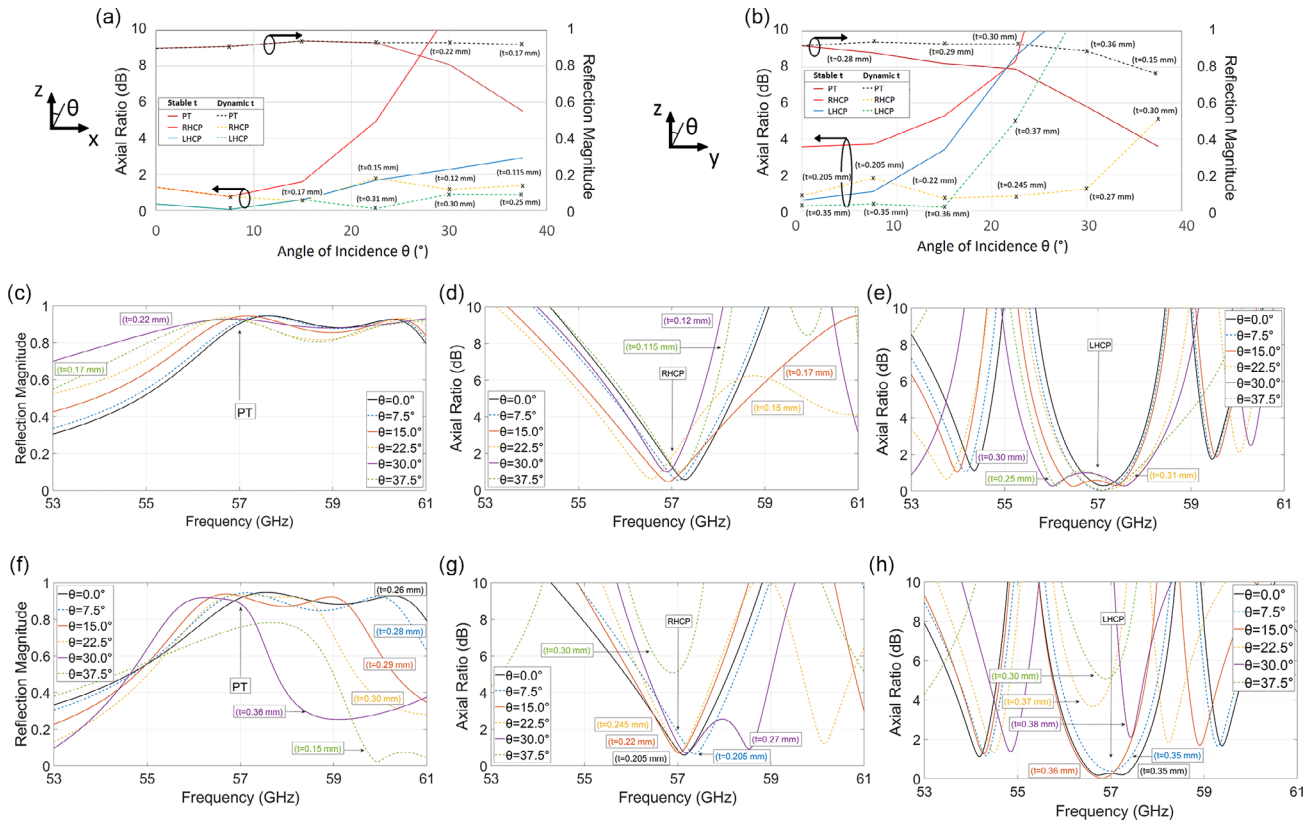


Figure 5. Angular stability study. Comparison of the axial ratio and reflection magnitude is presented for a stable ground plane position (RHCP: 0.19 mm, PT: 0.26 mm, and LHCP: 0.34 mm) and a variable ground plane for different angles of incidence a) θ_{zx} and b) θ_{zy} . The dynamic nature of the device allows us to satisfy the three functions c) polarization twist, d) RHCP, and e) LHCP for different values of θ_{zx} and the same three functions f) polarization twist, g) RHCP, and h) LHCP for different values of θ_{zy} .

height was selected so that we have a polarization conversion at around 57 GHz. The initial values of the cavity height values are 0.26, 0.19, and 0.34 mm, respectively. An important feature of the structure is that the ground plane can be moved dynamically, so we can adjust it according to the angle of incidence to maintain the structure's performance. Figure 5a,b shows the structure's performance at 57 GHz for a fixed position of the ground plane and for a dynamic change of the ground plane for scanning the angles θ_{zx} and θ_{zy} . For angle θ_{zx} scanning, we can maintain a stable performance for all functions up to 37.5° by dynamically shifting the ground plane. The dynamic movement of the ground plane significantly improves the structure's operation compared to the fixed ground plane. Regarding the scanning of the angle θ_{zy} , although it improves significantly with the dynamic change of the ground plane, we cannot maintain the conversion of the linear polarization to left-handed circular for more than 15°. The conversion of linear polarization to right-handed circular and the rotation of linear polarization can be maintained up to an angle θ_{zy} of 30°.

The stability of the structure with respect to the change in the angle of incidence is determined by the less stable function in each plane. In this structure, the least robust function is converting linear polarization to left-handed circular polarization, which happens for angle θ_{zy} scanning as defined in Figure 5b. For scanning angle θ_{zx} , the structure operates up to 37.5°, and for

scanning angle θ_{zy} , the structure operates up to 15°. The results for scanning the angle θ at the two planes are presented in detail in Figure 5c–h. In summary, we can assume that the stability of the structure with respect to changes in the angle of incidence is more inherent in the dynamic nature of the structure than in the configuration of the periodic array.

2.4. Fabricated Prototype

The fabricated dynamically tuneable prototype, as shown in **Figure 6**, consists of the periodic array, a ground plane, and a commercially available piezoelectric actuator, PiezoMove P-603.5S1 (by Physik Instrument Ltd UK). The ground plane is positioned at a distance t from the dielectric, creating the necessary cavity. In this arrangement, the substrate is not included in the cavity to minimize reflection losses and maximize the effect of cavity change. The proposed piezoelectric mechanism is attached to the ground plane, allowing the cavity to move vertically, which in turn provides the polarization control. Standard PCB fabrication was used for the periodic array. The substrate is the Nelco NY9220ST0787S1S1 with a thickness of 0.78 mm, which is commercially available and has a dielectric constant of 2.2 and a loss tangent of 0.0009. The periodic array surface is 120 mm², corresponding to $\approx 20\lambda \times 20\lambda$ for the lowest operating frequency.

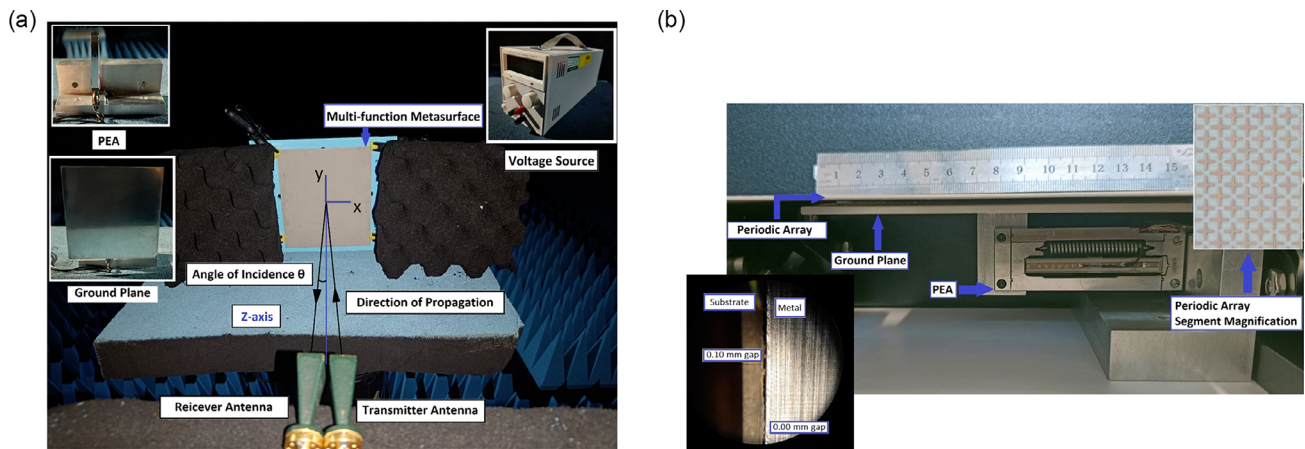


Figure 6. Experimental configuration. In a), the experimental configuration is illustrated. The two antennas are positioned in the far-field, and the polarizer is illuminated with TM polarization. To minimize the angle of incidence θ_xz , the two horn antennas are placed as close as possible to each other. The components (ground plane, PEA, and voltage source) behind the polarizers and the absorbers are depicted in the three inserts. b) The reconfigurable polarizer is depicted, and we highlight the different components. In the top right insert, we present a magnification of a segment of the periodic array. In the down left insert is a photograph of the device under the microscope. Due to the roughness and elasticity of the dielectric microcavities are formed between it and the ground plane. The microcavities can have a height of up to 0.10 mm.

The motion of the piezoelectric mechanism is along the z-axis, as shown in Figure 6a. The periodic structure was placed in a fixed position during the experimental process. The piezoelectric mechanism was attached to the ground plane and placed behind the periodic array. As the initial position of the ground plane, we set its contact with the periodic array; this also ensures that the two parts are aligned. We do not apply voltage to the piezoelectric mechanism (0 V) in the initial position. Additional components used for the experimental validation of the structure were the voltage source that controls the piezoelectric actuator and a frame that holds the periodic array. Two standard gain horn antennas were placed opposite the structure in the far-field after the VNA was first calibrated. For the measurement, we tried to minimize the distance between the antennas and the angle θ of incidence to approach the normal incidence. By applying a voltage through the voltage source to the piezoelectric mechanism, we linearly and accurately remove the ground plane from the periodic array along the z-axis. The maximum voltage applied to the piezoelectric mechanism is 120 V, providing a displacement of up to 0.50 mm.

The Nelco NY9220ST0787S1S1 dielectric is rough and flexible. The result of this dielectric's characteristics is that microcavities are formed between the ground plane and the periodic array when they are in contact, which can be from 0.00 to 0.10 mm thick, as shown in Figure 6b. The specific characteristics do not affect the operation of the structure, as will be seen from the experimentally confirmed results.

The experimental process described was for measuring one orthogonal polarization; for the perpendicular orthogonal polarization, the structure was rotated by 90° to the x-axis. The reflection characteristics for both positions of the periodic array for the various applied voltages, which correspond to a variable distance between the ground plane and the periodic structure, are shown in Figure 7.

Figure 7a shows the voltage–displacement curve of the piezoelectric mechanism measured under a microscope. Figure 7b,c

shows the reflection losses for the periodic array's initial position and its rotation by 90° with respect to the x-axis; from 53 to 59 GHz, the losses are below 4 dB and are similar in both polarizations allowing the linear polarization to be converted.

Figure 7d,e shows the normalized reflection phase for various voltages with respect to the 0 V reflection phase for the two orthogonal linear polarizations. Although we tried to minimize the angle of incidence θ to approximate the normal incidence, we could not eliminate it. Also, we need to consider that the electric field might have an inclination of a few degrees with respect to the x-axis due to alignment tolerances.

We compare the experimented retrieved data with the normal incidence, which is why we have this small deviation in the phase between the simulations and the measurements. Figure 7f shows the phase difference between the two orthogonal polarizations where we observe that the phase differences of 0° , 90° , 180° , and 270° that are necessary for the four functions of the structure are satisfied. Additionally, it can be noted that for a constant distance between the ground plane and the periodic array, different polarization conversions can be observed at different frequencies.

Figure 7g presents the device's cross-polarization when illuminated by an electromagnetic wave with a linearity of 45° with respect to the y-axis. There is a good agreement between measurements and simulations if we take into account the 2 dB additional losses between measurements and simulations and the small deviations in angles θ and φ with respect to the z and x axes, respectively. A moving average filter was applied to the $|S_{21}|$ data to reduce noise caused by standing waves formed as a result of the test horn antennas being placed in close proximity to one another and in close proximity to the metasurface. The raw data are presented in the insert. Finally, in Figure 7h, we present the axial ratio for two different voltage values, which correspond to different functions of the device (RHCP and LHCP), and we compare it with simulations. The extra losses don't affect

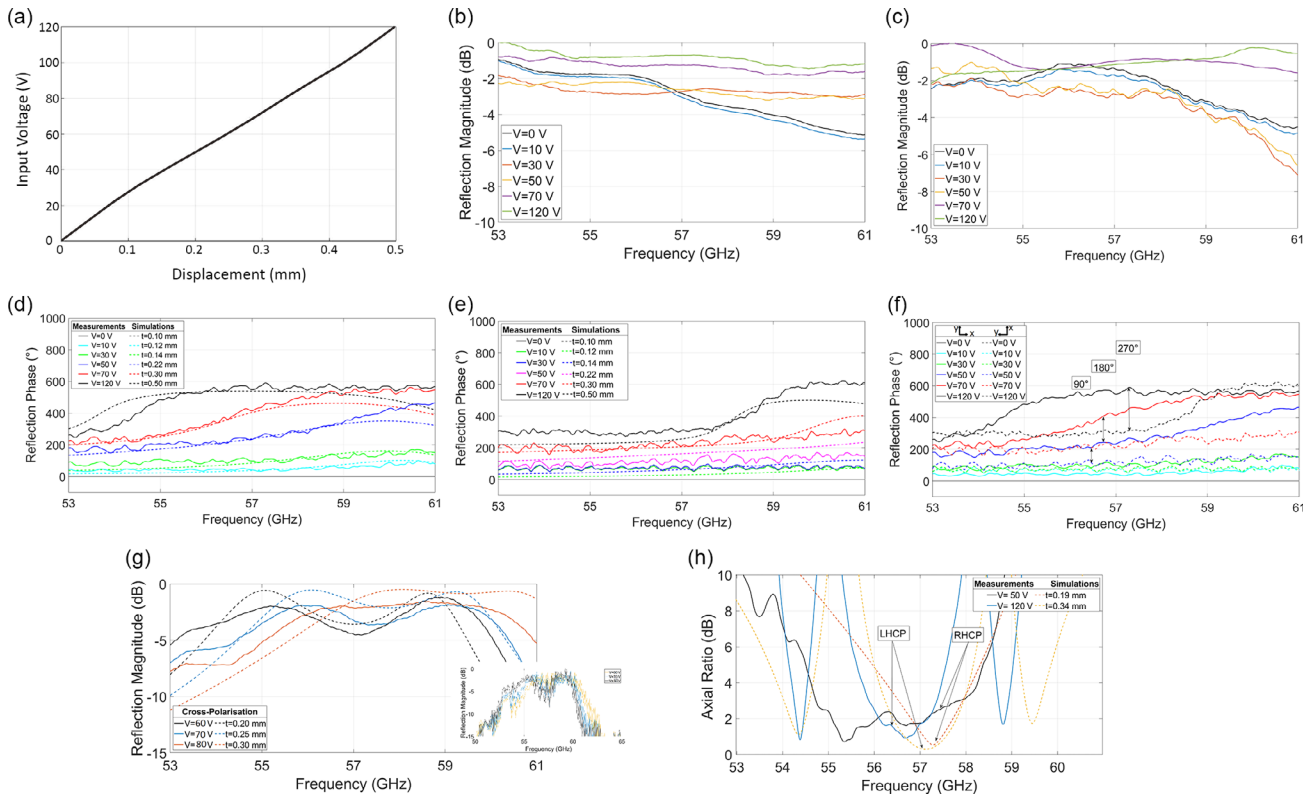


Figure 7. Experimental results. a) The displacement that provides the PiezoMove P-603.5S1 was measured by microscope. b) The device's reflection magnitude for the one orthogonal component of the electric field and c) the reflection magnitude for the perpendicular orthogonal component of the electric field. In d,e) are presented the simulated and measured reflection phase shift with respect to $t = 0.00$ mm and $V = 0$ V, respectively, for the two orthogonal components of the electric field. f) Comparison between d) 7 and e) 7 highlights the phase difference variation between them. The table legend presents the orientation of the periodic array. g) Measured and simulated cross-polarization when the device was illuminated with a linearity of 45° for different applications of voltage and different positions of the ground plane (raw data shown in insert). h) Measured and simulated axial ratio for different applied voltage and positions of the ground plane, highlighting the RHCP and the LHCP.

the axial ratio as they occur in the initial position of the periodic array and when it is rotated by 90° with respect to the x -axis.

3. Conclusion

Techniques that allow the tuning of *meta*-surfaces offer extensive possibilities for manipulating the spectral and spatial properties of electromagnetic waves. One of the essential characteristics of the electromagnetic wave is polarization. Its control is necessary for several applications, such as satellite communications and the automotive industry. Low-profile structures that control the polarization states would be critical to enhancing systems' flexibility and reducing costs.

In this manuscript, we introduce a new contribution to the state-of-the-art that utilizes piezoelectric tuning and extend the current possibilities of tuneable metasurfaces. This structure has two specific advantages. First, it introduces the maintenance of the polarization of the incident electromagnetic wave, which was not previously possible in combination with all the other three functions described earlier, and second, the low reflection loss performance which is particularly challenging at mm-waves.

The active mechanism is shielded below the ground plane and does not interact with the electromagnetic wave as with any other mechanism, so no additional losses are introduced. This allows this type of metasurface to operate at millimeter frequencies as well as being particularly scalable to even higher frequencies up to the THz band.

Traditional tuning mechanisms, integrated into structures at higher frequencies, show increased losses. In the case of the piezoelectric actuator, as we proceed to higher frequencies, its capabilities increase as the amount of available displacement becomes a larger fraction of the wavelength, thus, it can lead to an increased operating range. The limitations of this mechanism for operating frequency come only from the positional accuracy of about $1 \mu\text{m}$ sufficient to provide continuous tuning into the THz region.

This manuscript presents a structure that gives complete freedom regarding the conversion of linear polarization and is confirmed experimentally. The structure has a dynamic operating range for normal incidence ranging from 53.8 to 59 GHz, with each function having at least 0.5 GHz constant bandwidth for each ground plane position. The four functions are the conversion of the linear polarization to a right-handed circular

polarization, left-handed circular polarization, its rotation by 90°, and finally, its polarization maintenance. If we want to consider a range of operations in which the structure performs despite the changes in the angle of incidence, we can consider that it is from 56.5 to 57.5 GHz to maintain its functions.

The displacement of the PEA varies continuously with applied voltage but can suffer from hysteresis effects. To experimentally control the piezoelectric mechanism, we must apply voltage from 0 to 120 V to achieve a shift from 0 to 0.50 mm. This study prevented the hysteresis effect by unidirectional voltage application after initial calibration. Also, commercially available actuators have closed-loop feedback control electronics to avoid hysteresis effects.

The piezoelectric actuator, PiezoMove P-603.5S1, is superior in terms of switching speeds in combination with the required displacement compared to any other moving mechanism such as solenoids, small motors, or other magnetic-based devices. The speed of the aforementioned actuators is typically in the order of a few milliseconds and varies depending on load. Based on the weight of the ground plane micromachined for this experiment, a switching speed of less than 2 ms could be expected. Additionally, the durability of the actuator exceeds 10^9 cycles which is superior to any other mechanism that provides this displacement. The limitation of the piezo-tuning systems is the alignment tolerance, but we can overcome them with modern ultra-high precision manufacturing, metrology, and automated optical instruments.

Future research aims to investigate the potential for enhancing the structure's operating bandwidth and reducing losses by altering the configuration of the periodic array. In addition, an attempt will be made to integrate this *meta*-surface into antennas to create a compact antenna that can change its polarization.

4. Experimental Section

Piezoelectric Actuator: The PEA tuning technique uses the reverse piezoelectric effect whereby a piezoelectric material with an applied charge across its volume will produce a mechanical strain. With the commercially sourced PEAs used in these experiments, numerous thin disks of the piezoelectric material, namely lead zirconate titanate (PZT), are formed into a stack and biased via interleaved electrodes. When a biasing voltage is applied, the stack translates the resulting strain into an increase in the overall stack length. The stack is constrained within an aluminum flexure assembly, which acts as a lever and amplifies the increase in length to a maximum lateral travel distance of ≈ 20.50 mm. The PEA encased in the flexure assembly can be seen in Figure 6b. The PEA used in the presented studies is the PiezoMove P-603.5S1 (by Physik Instrumente Ltd. UK)^[54] with dimensions $2\text{ cm} \times 6\text{ cm} \times 0.6\text{ cm}$, and the moving part was oriented perpendicular to the ground plane and attached to provide lateral movement.

The application of the voltage between 0 and 120 V controls the position of the PEA head for a displacement between 0 and 0.50 mm. The manufacturer asserts that the actuator offers a movement resolution of 5 nm and a linear movement error of 0.2%. A displacement–voltage graph is shown in Figure 7a. This graph does not show the effects of hysteresis, but with the unidirectional application of voltage, this graph was consistent as observed and recorded by a measurement microscope.

Data Extraction: The presented experiment was set up so that two standard gain horn antennas of appropriate bandwidth and minimal incidence angle were configured to detect reflected S21 magnitude and phase in the far-field, as shown in Figure 6a. Bare ground measurements were also

taken with the periodic surface absent so that free path losses may be removed to isolate the effects of the metasurface. A moving average filter was applied to the |S21| data to reduce noise caused by standing waves formed as a result of the test horn antennas being placed in close proximity to one another and in close proximity to the device under test. The proximity of the antennas was required to minimize the angle of incidence for the reflection measurements desired for the intended use of this reconfigurable polarizer.

The metasurface was first designed and optimized for its particular objectives in an industry-standard EM simulation package (CST Microwave Studio). Individual unit cells were simulated using periodic boundary conditions, which yield the result of an infinite array of unit cell designs and are commonly used to model array sizes over $20\lambda \times 20\lambda$ under plane wave incidence with very good accuracy. The PEA component was not required during the simulation, as it does not form part of the EM system. Its effect was modeled by directly varying the air gap between the periodic surface and ground plane.

Fabrication and Equipment: For experimental validation, standard PCB methods were sourced using a Nelco NY9220ST0787S1S1 substrate with a dielectric constant of 2.2, loss tangent of 0.0009, and thickness of 0.78 mm. The metasurface printed on the substrate had dimension $20\lambda \times 20\lambda$ at the lowest frequency which should provide a similar result to an infinite surface simulation. The device is presented in Figure 6b. The periodic array was brought in contact with the variable ground plane for testing. The PEA was connected to a DC voltage source to control the displacement. By increasing the voltage, the ground plane moved away from the surface, and the air cavity height increased. A ZVA 67 A vector network analyzer (Rohde & Schwarz) was used to sweep the appropriate frequency ranges. Specialized phase-stable cables (ZV.796) were used to ensure accurate reporting of phase measurements.

Acknowledgements

Department of Electrical, Electronic and Systems Engineering, University of Birmingham, Birmingham, B15 2SA, UK.

Conflict of Interest

The authors declare no conflict of interest.

Data Availability Statement

The data that support the findings of this study are available from the corresponding author upon reasonable request.

Keywords

millimeter-waves, piezoelectric actuators, polarization control, tunable metasurfaces

Received: March 21, 2023

Revised: May 11, 2023

Published online:

- [1] F. Falcone, T. Lopetegui, M. A. G. Laso, J. D. Baena, J. Bonache, M. Beruete, R. Marques, F. Martin, M. Sorolla, *Phys. Rev. Lett.* **2004**, *93*, 197401.
- [2] X. G. Luo, *Sci. China Phys. Mech. Astron.* **2015**, *58*, 594201.
- [3] N. I. Zheludev, Y. S. Kivshar, *Nat. Mater.* **2012**, *11*, 917.
- [4] H. B. Wang, Y. J. Cheng, Z. N. Chen, *IEEE Trans. Antennas Propag.* **2021**, *69*, 9021.

- [5] H. B. Wang, Y. J. Cheng, *IEEE Trans. Antennas Propag.* **2019**, *67*, 4296.
- [6] Z. Li, W. Liu, H. Cheng, S. Chen, J. Tian, *Sci. Rep.* **2015**, *5*, 18106.
- [7] S. Sun, Q. He, S. Xiao, Q. Xu, X. Li, L. Zhou, *Nat. Mater.* **2012**, *11*, 426.
- [8] S. Sun, K. Y. Yang, C. M. Wang, T. K. Juan, W. T. Chen, C. Y. Liao, Q. He, S. Xiao, W. T. Kung, G. Y. Guo, L. Zhou, D. P. Tsai, *Nano Lett.* **2012**, *12*, 6223.
- [9] J. P. Gianvittorio, Y. Rahmat-Samii, *IEEE Trans. Antennas Propag.* **2006**, *54*, 1388.
- [10] A. Ahmadi, S. Ghadarghad, H. Mosallaei, *Opt. Express* **2010**, *18*, 123.
- [11] K. K. Kishor, S. V. Hum, *IEEE Trans. Antennas Propag.* **2012**, *60*, 197.
- [12] M. A. Kats, D. Sharma, J. Lin, P. Genevet, R. Blanchard, Z. Yang, M. M. Qazilbash, D. N. Basov, S. Ramanathan, F. Capasso, *Appl. Phys. Lett.* **2012**, *101*, 221101.
- [13] S. Chejarla, S. R. Thummaluru, S. Kalraiya, R. K. Chaudhary, in *2018 3rd Int. Conf. on Microwave and Photonics (ICMAP) 2018*, pp. 1–2.
- [14] B. Zhu, Y. Feng, J. Zhao, C. Huang, T. Jiang, *Appl. Phys. Lett.* **2010**, *97*, 051906.
- [15] A. P. Feresidis, G. Goussetis, S. Wang, J. C. Vardaxoglou, *IEEE Trans. Antennas Propag.* **2005**, *53*, 209.
- [16] K. Sun, C. A. Riedel, Y. Wang, A. Urbani, M. Simeoni, S. Mengali, M. Zalkovskij, B. Bilenberg, C. H. de Groot, O. L. Muskens, *ACS Photonics* **2018**, *5*, 495.
- [17] C. Pfeiffer, A. Grbic, *IEEE Trans. Microw. Theory Tech.* **2013**, *61*, 4407.
- [18] J. Y. Lau, S. V. Hum, *IEEE Trans. Antennas Propag.* **2012**, *60*, 5679.
- [19] M. Selvanayagam, G. V. Eleftheriades, *IEEE Trans. Microw. Theory Tech.* **2016**, *64*, 414.
- [20] H. X. Xu, G. Hu, Y. Wang, C. Wang, M. Wang, S. Wang, Y. Huang, P. Genevet, W. Huang, C. W. Qiu, *Light Sci. Appl.* **2021**, *10*, 75.
- [21] H.-X. Xu, Y. Wang, C. Wang, M. Wang, S. Wang, F. Ding, Y. Huang, X. Zhang, H. Liu, X. Ling, W. Huang, *Research* **2021**, 2021, <https://doi.org/10.34133/2021/6382172>.
- [22] H. X. Xu, S. Tang, G. M. Wang, T. Cai, W. Huang, Q. He, S. Sun, L. Zhou, *IEEE Trans. Antennas Propag.* **2016**, *64*, 3676.
- [23] H. X. Xu, G. Hu, L. Han, M. Jiang, Y. Huang, Y. Li, X. Yang, X. Ling, L. Chen, J. Zhao, C. W. Qiu, *Adv. Opt. Mater.* **2019**, *7*, 1801479.
- [24] H. T. Chen, A. J. Taylor, N. Yu, *Rep. Progr. Phys.* **2016**, *79*, 076401.
- [25] E. A. Parker, S. B. Savia, *IEEE Proc. Microwaves Antennas Propag.* **2001**, *148*, 103.
- [26] G. Perez-Palomino, P. Baine, R. Dickie, M. Bain, J. A. Encinar, R. Cahill, M. Barba, G. Toso, *IEEE Trans. Antennas Propag.* **2013**, *61*, 1704.
- [27] G. Perez-Palomino, M. Barba, J. A. Encinar, R. Cahill, R. Dickie, P. Baine, M. Bain, *IEEE Trans. Antennas Propag.* **2015**, *63*, 3722.
- [28] M. R. M. Hashemi, S. H. Yang, T. Wang, N. Sepúlveda, M. Jarrahi, *Sci. Rep.* **2016**, *6*, 35439.
- [29] S. R. Biswas, C. E. Gutiérrez, A. Nemilentsau, I. H. Lee, S. H. Oh, P. Avouris, T. Low, *Phys. Rev. Appl.* **2018**, *9*, 034021.
- [30] H. X. Xu, S. Sun, S. Tang, S. Ma, Q. He, G. M. Wang, T. Cai, H. P. Li, L. Zhou, *Sci. Rep.* **2016**, *6*, 27503.
- [31] D. F. Sievenpiper, J. H. Schaffner, H. Jae Song, R. Y. Loo, G. Tangonan, *IEEE Trans. Antennas Propag.* **2003**, *51*, 2713.
- [32] H. X. Xu, S. Tang, S. Ma, W. Luo, T. Cai, S. Sun, Q. He, L. Zhou, *Sci. Rep.* **2016**, *6*, 38255.
- [33] E. Vassos, J. Churm, J. Powell, C. Viegas, B. Alderman, A. Feresidis, *Sci. Rep.* **2021**, *11*, 5988.
- [34] J. M. Zendejas, J. P. Gianvittorio, Y. Rahmat-Samii, J. W. Judy, *J. Microelectromech. Syst.* **2006**, *15*, 613.
- [35] L. Cong, P. Pitchappa, C. Lee, R. Singh, *Adv. Mater.* **2017**, *29*, 1700733.
- [36] E. Vassos, J. Churm, A. Feresidis, *Sci. Rep.* **2020**, *10*, 15679.
- [37] M. Mavridou, A. P. Feresidis, *IEEE Trans. Antennas Propag.* **2016**, *64*, 5190.
- [38] J. I. Herranz-Herruzo, A. Valero-Nogueira, M. Ferrando-Rocher, B. Bernardo, A. Vila, R. Lenormand, *IEEE Trans. Antennas Propag.* **2018**, *66*, 2661.
- [39] P. W. Gaiser, K. M. St. Germain, E. M. Twarog, G. A. Poe, W. Purdy, D. Richardson, W. Grossman, W. L. Jones, D. Spencer, G. Golba, J. Cleveland, L. Choy, R. M. Bevilacqua, P. S. Chang, *IEEE Trans. Geosci. Remote Sens.* **2004**, *42*, 2347.
- [40] J. G. Chang, M. Shoshany, Y. Oh, *IEEE Trans. Geosci. Remote Sens.* **2018**, *56*, 7102.
- [41] K. Sarabandi, *IEEE Trans. Microw. Theory Tech.* **1994**, *42*, 2171.
- [42] S. Hollung, W. Shiroma, M. Marković, Z. B. Popović, *IEEE Microwave Guid. Wave Lett.* **1996**, *6*, 205.
- [43] T. Manabe, J. Inatani, A. Murk, R. J. Wylde, M. Seta, D. H. Martin, *IEEE Trans. Microw. Theory Tech.* **2003**, *51*, 1696.
- [44] A. Sims, T. Freialdenhoven, T. Dallmann, in *2020 50th European Microwave Conf. (EuMC)*, **2021**, pp. 571–574.
- [45] J. A. Ruiz-Cruz, M. M. Fahmi, M. Daneshmand, R. R. Mansour, in *2011 IEEE MTT-S Int. Microwave Symp.*, IEEE, Piscataway, NJ **2011**, pp. 1–4.
- [46] J. A. Ruiz-Cruz, M. M. Fahmi, S. A. Fouladi, R. R. Mansour, *IEEE Trans. Microw. Theory Tech.* **2011**, *59*, 3365.
- [47] E. Doumanis, G. Goussetis, R. Dickie, R. Cahill, P. Baine, M. Bain, V. Fusco, J. A. Encinar, G. Toso, *IEEE Trans. Antennas Propag.* **2014**, *62*, 2302.
- [48] P. Y. Wang, B. Sievert, J. T. Svejda, N. Benson, F. Y. Meng, A. Rennings, D. Erni, *IEEE Trans. Antennas Propag.* **2023**, *71*, 1135.
- [49] N. Tentillier, F. Krasinski, R. Sauleau, B. Splingart, H. Lhermite, P. Coquet, *IEEE Antennas Wirel. Propag. Lett.* **2009**, *8*, 701.
- [50] A. Ptilakis, M. Seckel, A. C. Tasolamprou, F. Liu, A. Deltsidis, D. Manassis, A. Ostmann, N. V. Kantartzis, C. Liaskos, C. M. Soukoulis, S. A. Tretyakov, M. Kafesaki, O. Tsilipakos, *Phys. Rev. Appl.* **2022**, *17*, 064060.
- [51] T. Li, R. Wang, J. Sun, W. Dou, *IEEE Antennas Wirel. Propag. Lett.* **2022**, *21*, 2254.
- [52] E. Doumanis, G. Goussetis, J. L. Gómez-Tornero, R. Cahill, V. Fusco, *IEEE Trans. Antennas Propag.* **2012**, *60*, 212.
- [53] C. A. Balanis, *Antenna Theory: Analysis and Design*, 4th ed., Wiley **2016**.
- [54] Physik Instrumente UK, <http://www.physikinstrumente.co.uk> (accessed: June 2023).